Supporting Information

Hennig et al. 10.1073/pnas.1117126109

SI Materials and Methods

Materials. All chemicals were purchased from Sigma, Fermentas, AppliChem, and Roth and were of at least analytical grade. N_2 and N_2/H_2 (95%/5%) gases were obtained from Air Liquide. Enzymes (DNA polymerases, DNA ligases, and restriction enzymes) used in molecular biology were purchased from either Fermentas or Finnzymes (Thermo Fisher). Corrinoid-iron/sulfur protein (CoFeSP) was heterologously produced as described recently (1). All anaerobic solutions were prepared in bottles with butyl rubber septum by successive cycles (at least four cycles) of evacuating and flushing with N_2 gas at a vacuum-gas line. Purification, crystallization, and all other biochemical experiments were performed under anaerobic conditions under an atmosphere of 95% N_2/5% H_2 inside a glove box (model B; COY Laboratory Products, Inc.).

Cloning, Site-Directed Mutagenesis, and Expression. The gene CHY_1224 located in the gene cluster coding for the structural genes of the reductive acetyl-CoA pathway, was amplified by PCR from the genomic DNA of *Carboxydothermus hydrogenoformans* Z-2901 using Phusion DNA polymerase (Finnzymes) and a primer pair containing NdeI and XhoI restriction sites. A 1,896 bp DNA fragment was digested by NdeI/XhoI and ligated into an NdeI/XhoI-digested pETDuet1 vector (Novagen). After transformation of the ligation products into *Escherichia coli* DH5α, a positive plasmid was analyzed by DNA sequencing (Eurofins) and named pPKCoDuet1.

For a simplified purification of the designed single mutants of the activator, the plasmid pPKCoDuet1 was modified by inserting a cleavage site (ENLYFQG) for Tobacco Etch Virus (TEV) protease in the Multiple Cloning Site 1, sequenced and named pPKCoDuet1TEV. Single amino acids of the activator were exchanged by the quick-change method with the pPKCoDuet1TEV as a template and primer pairs for the desired mutants using *Pfu* DNA polymerase (Fermentas). The amplified DNA product was digested with DpnI and transformed into *E. coli* DH5α. Positive plasmids for each mutant were identified by DNA sequencing and named pPKCoDuet1TEV-D212A, pPKCoDuet1-TEV-D377A, and pPKCoDuet1TEV-E404A.

For the expression of the wild-type protein and the mutants D212A, D377A, and E404A, the plasmids pPKCoDuet1, pPKCo-Duet1TEV-D212A, pPKCoDuet1TEV-D377A, and pPKCo-Duet1TEV-E404A were transformed into the *E. coli* strain BL21 (DE3). The cultures were grown at 37 °C by shaking in modified TB media (2) supplemented with carbenicilin (100 μg/mL), 0.3 mM $FeSO_4$, and 0.3 mM Na_2S. When the OD_{600} of the culture reached 0.7–0.8, it was induced by the addition of 0.2 mM isopropyl β-D-thiogalactopyranoside and supplemented with 0.3 mM $FeSO_4$ and 0.3 mM Na_2S. The culture was further fermented for 6 h at 32 °C after induction, before it was harvested. Cell pellets were stored at −20 °C until use.

Purification of the Wild Type and Mutants of the Reductive Activator of CoFeSP (RACo). All steps were carried out anaerobically inside a glove box (model B; COY Laboratory Products, Inc.). Frozen cells were resuspended in buffer A (50 mM Tris•HCl, pH 8.0 and 2 mM DTT) and broken in an ice-cooled glass rosette by sonication. The suspension of broken cells was cleared from cell debris by ultracentrifugation at $142,400 \times g$ and 8 °C for 1 h.

The supernatant containing the wild-type protein was loaded on a DEAE column (50 mL) equilibrated with buffer A, followed by washing with the same buffer. Protein was eluted with 500 mL of a linear gradient of 0–1 M NaCl in buffer A. Reddish-brown colored fractions were pooled and suspended in a 1 M ammonium sulfate solution, stirred for 1 h, and centrifuged at $12,100 \times g$ and 8 °C for 15 min. The supernatant was applied to a phenyl sepharose column (22 mL) equilibrated with buffer A containing 1 M ammonium sulfate. Proteins were eluted by applying a 300 mL linear gradient of 1–0 M ammonium sulfate in buffer A. Reddish-brown colored fractions containing the target protein were combined and concentrated to a volume of less than 5 mL using a spin concentrator Vivaspin 70 (50 kDa molecular weight cutoff; Vivascience GmbH) equipped with a rubber-sealed screw cap. Concentrated wild-type RACo was loaded on a 120 mL Superdex™ 200 prep-grade gel filtration column (GE Healthcare) equilibrated in buffer A containing 150 mM NaCl. The fractions corresponding to the size of the dimer (approximately 160 kDa) were collected. The protein solution was concentrated and frozen in glass vials equipped with butyl rubber septum in liquid N_2 and stored at −80 °C.

To purify the three enzyme variants, the supernatant containing the desired variant was loaded on a Ni-sepharose high-performance column (5 mL) equilibrated with buffer A containing 20 mM imidazole and 200 mM NaCl. The tightly bound protein fraction was eluted using buffer A containing 250 mM imidazole and 200 mM NaCl. After buffer exchange to buffer A containing 150 mM NaCl by a prepacked desalting G25 column, the His_6 tag of the mutated protein was removed by overnight incubation at room temperature with His_6-tagged TEV protease in the same buffer supplemented with 5 mM β-mercaptoethanol. To separate cleaved His_6 tag and TEV protease from the tag-cleaved protein, the solution was loaded on the Ni-sepharose high-performance column, the flow-through fraction was collected and concentrated to a volume less than 2 mL using a spin concentrator Amicon Ultra-15 30 K (Millipore). The concentrated protein solution was loaded on a Superdex™ 200 prep-grade gel filtration column and the same protocol as used in the wild-type purification was applied to finalize the purification of the mutated proteins.

Analytical Procedures. Non-heme iron content of the as-isolated RACo was determined by the published method of Fish (3). Protein concentrations were routinely measured after Bradford (4) using the Roth reagent (Roti®-Quant).

UV-Visible (UV-vis) Spectroscopy. UV-vis spectra of RACo wild type and the mutants were measured on an Agilent 8453 photodiode array spectrophotometer. All measurements were performed anaerobically at room temperature using quartz cuvettes with 1 cm path length. The UV-vis spectrum of 4 μM RACo (as-isolated) in buffer A was recorded. To obtain reduced RACo, 2 mM dithiothreitol (DTT reduced) were added and the complete reduction was achieved after 10 min incubation.

ATPase Activity Assay. The hydrolysis of ATP catalyzed by RACo was measured anaerobically with a coupled assay using pyruvate kinase (PK) and lactate dehydrogenase (LDH) (5). The reaction mixture was prepared in buffer B (50 mM Hepes, 150 mM K-acetate, and 8 mM Mg-acetate adjusted to pH 7.5 by KOH) and contained 2 mM phosphenolpyruvate, 9.9 units LDH, 6.8 units PK, and 200 nM RACo. Between 0.2 and 5 μM of CoFeSP were included in the reaction mixture to test the influence of CoFeSP on the ATPase activity of RACo. This solution served as a blank before 0.16 mM NADH was added. The reaction was initiated by adding ATP to the reaction mixture. The decrease of NADH

absorption at 340 nm was followed at a constant temperature of 25 °C (Agilent 8453 photodiode array spectrophotometer equipped with Peltier element). The rate of NADH consumption by LDH corresponds to the rate of ATP hydrolysis and was used to calculate the ATPase activity of RACo. The unit of ATPase activity was defined as micromoles of ADP production per minute. The steady-state kinetic constants, K_m and V_{max}, were determined by varying ATP concentrations from 0 to 9 mM. The program GraFit 5 (6) was used for nonlinear regression analysis applying the Michaelis–Menten equation.

ATP-Dependent Reductive Activation Assay. ATP-dependent electron transfer from RACo to Co(II)-CoFeSP was determined anaerobically at a constant temperature of 25 °C. The assay mixture contained 2 μM activator, 2 or 4 μM Co(II)-CoFeSP, and 2 mM DTT in a final volume of 500 μL in buffer B. The reduction of RACo by DTT was followed by the decrease of the absorption at 350, 410, and 460 nm. When the reduction was completed, a blank spectrum was taken to define the baseline. The ET from the reduced RACo to Co(II)-CoFeSP was initiated by adding ATP. The development of Co(I)-CoFeSP was followed by monitoring the increase of the absorption at 390 nm and the decrease of absorption at 475 nm on an Agilent 8453 photodiode array spectrophotometer. Spectra were recorded every 10 s. For the mutants, the same assay was applied using 2 and 10 μM of the mutants.

Complex Formation of RACo and CoFeSP. To investigate the complex formation between RACo and CoFeSP, we performed gel filtration experiments using a Superdex™ 200 prep-grade gel filtration column inside the glove box. Generally, 45 μM of each protein was dissolved in buffer A containing 150 mM NaCl, and incubated for 10 min before injection to the column. Incubating the protein with 5 mM ATP or 5 mM ADP in the presence of 50 mM $MgCl_2$ was used to test the influence of nucleotides on the formation of the complex. We determined complex formation of RACo with different states of CoFeSP [Co(I), Co(II), and CH_3-Co(III)]. Co(I)-CoFeSP was prepared by incubating Co(II)-CoFeSP with 1 mM Na-dithionite. The gel filtration experiment was run using the same buffer as before but containing 1 mM Na-dithionite. CH_3-Co(III)-CoFeSP was prepared by reconstitution of the [Fe/S]-only CoFeSP (1) with methyl-cobalamin instead of hydroxocobalamin. Individual peak fractions from each gel filtration experiment were collected for analysis by SDS-polyacrylamide gel electrophoresis. A densitometry analysis of the SDS gels was conducted using the program ImageMaster™ 2D Platinum v7.0 (GE Healthcare). The elution volumes of the peaks were transformed into molecular weights using a standard curve constructed from known standard proteins in the running buffer: 4 mg/mL lactate dehydrogenase (140 kDa), 4 mg/mL conalbumin (75 kDa), 4 mg/mL ovalbumin (43 kDa), 4 mg/mL ribonuclease (13.7 kDa). All experiments were performed at least twice with independently prepared protein samples.

Crystallization and Crystal Treatment. RACo was crystallized under anaerobic conditions inside a glove box at 17 °C. Crystals were obtained by hanging-drop vapor diffusion and were grown in 0.15 M Mg-formate and 15% (wt/vol) PEG 3350 with and without 40 mM Na-dithionite by mixing with an equivolume of the 20 mg/mL protein solution. The native crystals were harvested from 0.17 M Mg-formate and 17% (wt/vol) PEG 3350 and transferred to a harvesting solution by stepwise increasing of the Mg-formate and PEG 3350 concentrations. Crystals used for single isomorphous replacement combined with anomalous scattering (SIRAS) phasing were soaked in a solution containing 0.23 M Mg-formate, 23% (wt/vol) PEG 3350 and a saturated concentration of $HgCl_2$ for 30 min. Crystals were flash cooled in liquid N_2 by using a harvesting or a soaking solution containing 20% (vol/vol) glycerol as a cryoprotectant.

Data Collection, Phasing, and Structure Refinement. Diffraction data were collected at 100 K on an X-ray generator with rotating Cu-anode (Nonius FR591; Bruker AXS) for SIRAS phasing (native and $HgCl_2$ derivative) and at beamline BL 14.2 (BESSY, Berlin, Germany) to obtain a high-resolution dataset. To confirm the position of the [2Fe-2S] cluster, a dataset was collected at the high-energy side ($\lambda = 1.73$ Å) of the K-absorption edge of Fe for the calculation of an anomalous difference Fourier map.

Diffraction datasets were integrated and scaled using X-ray Detector Software (XDS) (7). Initial phases were calculated by SIRAS techniques from the datasets of native ($d_{min} = 2.35$ Å) and $HgCl_2$-derivatized ($d_{min} = 2.62$ Å) activator crystals using the AutoSol module of PHENIX (8). Binding sites for eight Hg^{2+} ions were detected (Table S1). Iterative cycles of model building and refinements were carried out with COOT (9) and CNS (10). A first model of the activator without N-terminal domain was refined at 2.35 Å with final R/R_{free} values of 0.226/0.273 (Table S1). The crystal structure of the activator including the N-terminal [2Fe-2S] cluster domain was solved by Patterson search techniques with the native structure of the activator as homologous search model using Phaser-MR integrated in PHENIX. Residues Cys38–Cys44 were modeled based on comparison to homologous structures of known stereochemistry because they were only weakly defined in the electron density. Secondary structures were assigned using STRIDE (11). Data collection and refinement statistics of the reported structures are given in Table 1. Coordinates and structure factors have been deposited in the Protein Data Bank (PDB ID 3ZYY).

1. Goetzl S, Jeoung JH, Hennig SE, Dobbek H (2011) Structural basis for electron and methyl-group transfer in a methyltransferase system operating in the reductive acetyl-CoA pathway. *J Mol Biol* 411:96–109.
2. Jeoung JH, Dobbek H (2007) Carbon dioxide activation at the Ni,Fe-cluster of anaerobic carbon monoxide dehydrogenase. *Science* 318:1461–1464.
3. Fish WW (1988) Rapid colorimetric micromethod for the quantitation of complexed iron in biological samples. *Methods Enzymol* 158:357–364.
4. Bradford MM (1976) Rapid and sensitive method for quantitation of microgram quantities of protein utilizing principle of protein-dye binding. *Anal Biochem* 72:248–254.
5. Lindsley JE (2001) Use of a real-time, coupled assay to measure the ATPase activity of DNA topoisomerase II. *Methods Mol Biol* 95:57–64.
6. Leatherbarrow RJ (2001) GraFit Version 5 (Erithacus Software, Horley, UK).
7. Kabsch W (1993) Automatic processing of rotation diffraction data from crystals of initially unknown symmetry and cell constants. *J Appl Crystallogr* 26:795–800.
8. Adams PD, et al. (2010) PHENIX: A comprehensive Python-based system for macromolecular structure solution. *Acta Crystallogr D Biol Crystallogr* 66:213–221.
9. Emsley P, Cowtan K (2004) Coot: Model-building tools for molecular graphics. *Acta Crystallogr D Biol Crystallogr* 60:2126–2132.
10. Brunger AT, et al. (1998) Crystallography & NMR system: A new software suite for macromolecular structure determination. *Acta Crystallogr D Biol Crystallogr* 54:905–921.
11. Heinig M, Frishman D (2004) STRIDE: A web server for secondary structure assignment from known atomic coordinates of proteins. *Nucleic Acids Res* 32:W500–W502.

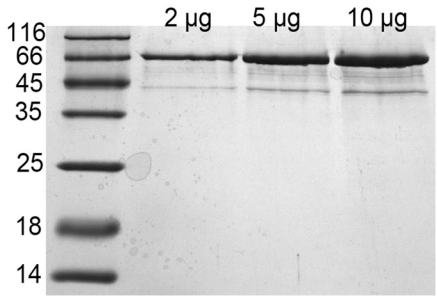

Fig. S1. SDS-PAGE analysis of the purification. The final activator fraction after three purification steps was loaded on a 12% (wt/vol) SDS gel to analyze protein purity. The first lane contains a molecular mass marker with the indicated sizes in kilodaltons. Concentrations of 2, 5, and 10 µg of the as-isolated protein are shown.

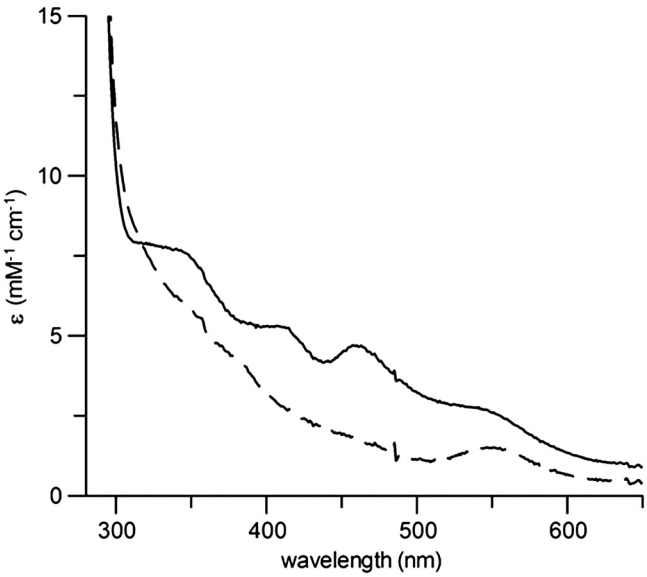

Fig. S2. UV-visible spectra of the activator. The as-isolated activator (solid line) showed absorption maxima at 350, 410, and 460 nm and a shoulder at 550 nm, which are characteristic for the presence of [2Fe-2S] clusters. The spectrum of reduced protein (dashed line) was obtained after incubating the as-isolated activator for 10 min with 2 mM DTT.

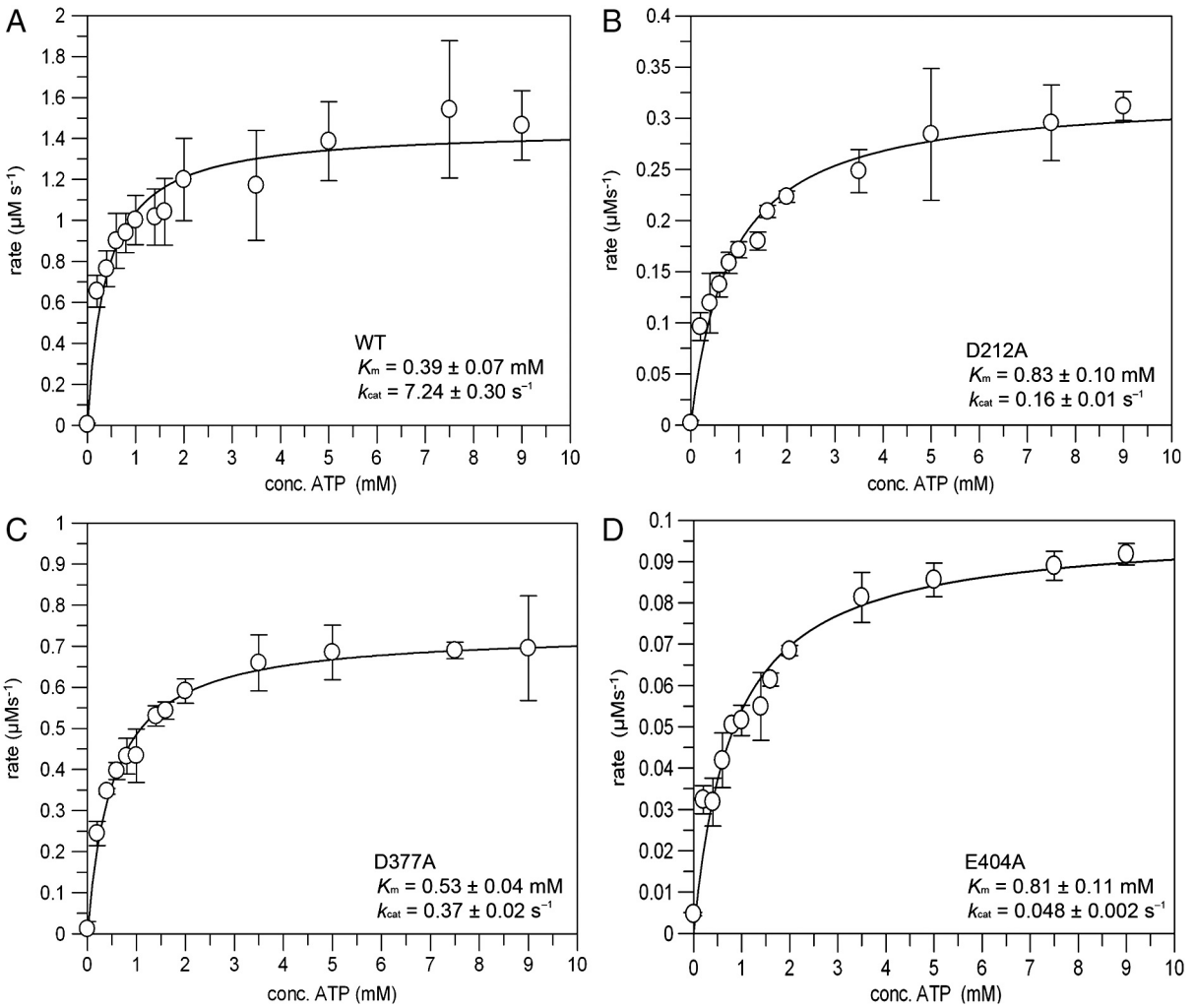

Fig. S3. Steady-state kinetics monitoring ATP hydrolysis. The rate of ATP hydrolysis was measured at different concentrations of ATP (0–9 mM) to determine the steady-state kinetic constants. Every measurement was performed in triplicate for all concentrations and standard derivations are shown. The steady-state kinetic constants for the wild-type [*A*, $K_m = 0.39 \pm 0.07$ mM and $V_{max} = 6.4 \pm 0.3$ μmol min^{-1} (mg of protein)$^{-1}$], for the D212A mutant [*B*, $K_m = 0.83 \pm 0.10$ mM and $V_{max} = 0.14 \pm 0.01$ μmol min^{-1} (mg of protein)$^{-1}$], for the D377A mutant [*C*, $K_m = 0.52 \pm 0.04$ mM and $V_{max} = 0.33 \pm 0.01$ μmol min^{-1} (mg of protein)$^{-1}$], and for the E404A mutant [*D*, $K_m = 0.81 \pm 0.11$ mM and $V_{max} = 0.043 \pm 0.002$ μmol min^{-1} (mg of protein)$^{-1}$] were calculated by nonlinear regression analysis with the Michaelis–Menten equation using the program GraFit 5 (6).

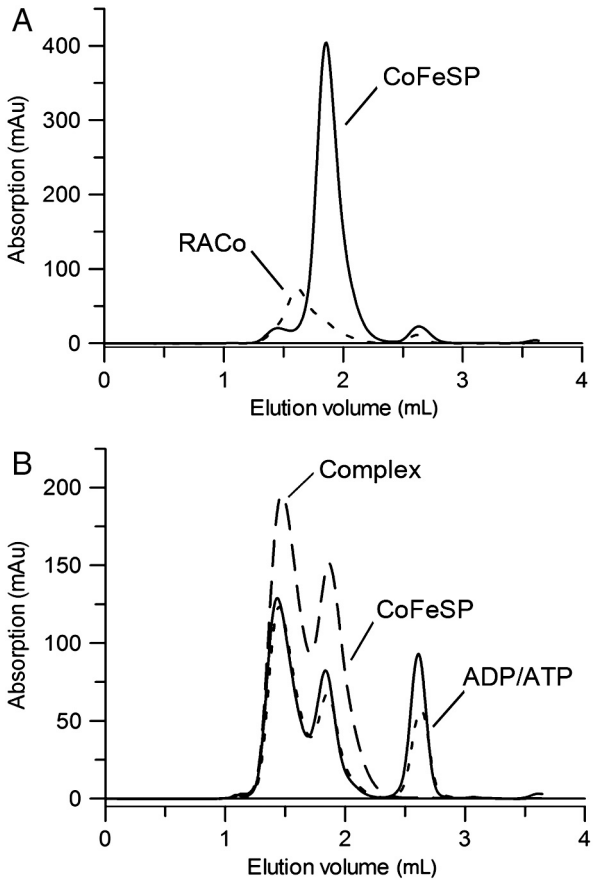

Fig. S4. Complex formation between CoFeSP and activator—influence of nucleotides and DTT. (*A*) Elution profile of the individual proteins. Activator (50 μM) and Co(II)-CoFeSP in 50 μL of a 50 mM Tris•HCl, pH 8.0, 150 mM NaCl, and 2 mM DTT were loaded separately on a Superdex S 150/5 analytical column (dimension 5 × 150 mm). The main peaks of RACo (dashed line) and CoFeSP (solid line) were visible at an elution volume (EV) of 1.61 and 1.86 mL, respectively. (*B*) Elution profile dependence on the redox state of activator and the presence of ADP or ATP. The two proteins were mixed and incubated 10 min prior to injection on the column. In the absence of DTT in the running buffer, the oxidized state of the activator formed a complex with Co(II)-CoFeSP (dashed line, EV = 1.46 mL). Irrespective of the presence of ADP (solid line, EV = 2.64 mL) or ATP (dotted line, EV = 2.65 mL), the complex between activator and Co(II)-CoFeSP was observed.

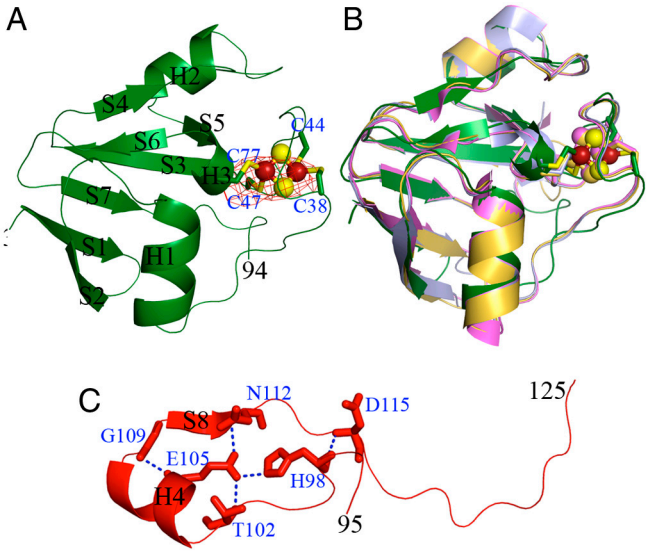

Fig. S5. N-terminal and linker domain. (*A*) The N-terminal domain containing the [2Fe-2S] cluster (residues 3–94). The four cysteine residues coordinating the iron atoms are shown as sticks. The [2Fe-2S] cluster in the N-terminal domain is depicted as spheres with iron in firebrick and sulfur in yellow. The anomalous difference Fourier map calculated using a dataset collected at the high-energy site of of the Fe-K edge (1.73 Å) is shown as a red-colored mesh contoured at 3σ. H3 is a 3_{10} helix. (*B*) Superposition of the N-terminal domain of the activator (same color as in *A*) with homologous plant-type [2Fe-2S] ferredoxins: in light blue, the heterocyst ferredoxin of *Anabaena* 7120 (PDB ID 1FRD); in yellow-orange, ferredoxin I from *Equisetum arvense* (PDB ID 1FRR); and in pink, the ferredoxin from *Synechocystis* (PDB ID 1OFF). (*C*) The linker domain consisting of one β-strand and one α-helix with residues from 95 to 125. H-bonding interactions stabilizing H4 with S8 are shown as blue dashed lines.

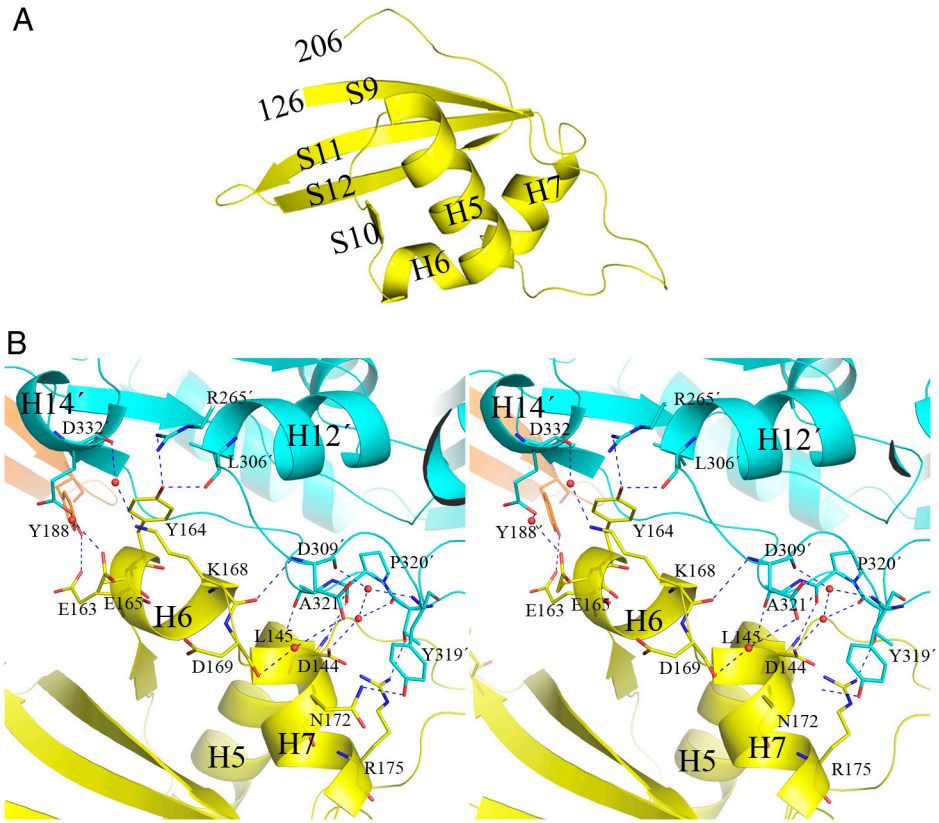

Fig. S6. Middle domain. (*A*) The middle domain shown in ribbon presentation. (*B*) Stereoview of the dimer interface. H-bonding interactions stabilizing the dimer interface of the activator are shown as blue dashed lines. The middle domain of one molecule is colored in yellow and the other middle domain of the dimer in orange. The ASKHA (acetate and sugar kinases/heat shock protein 70/actin) domain of subunit B (Fig. 3*A*) is depicted in cyan, and the residues and helices from subunit B are indicated by primes. Water molecules mediating H-bonding interactions are shown as spheres.

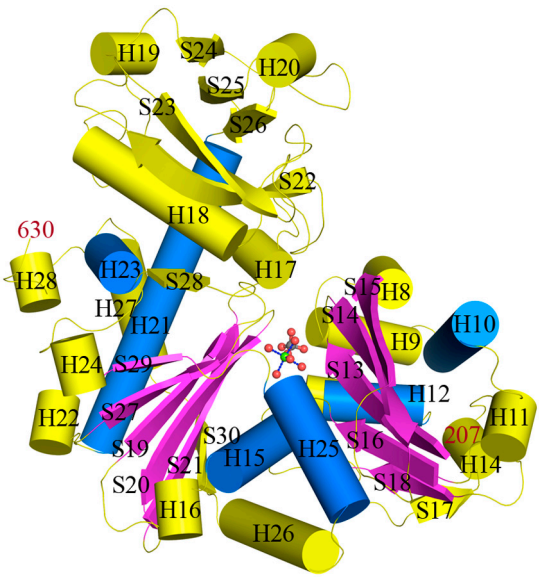

Fig. S7. ASKHA (acetate and sugar kinases/heat shock protein 70/actin) domain. Cartoon-representation of the ASKHA domain (residues 207–630). The conserved ββββαβαβα topology of the ASKHA family is shown with β-strands in magenta and α-helices in marine. H10, H13 (situated behind H12), H15, H16, H18, H19, H21, H23, H27 are 3_{10} helices. This core topology of the activator has an order of S13-S14-S15-H10-S16-H12-S18-H25 in domain I and S19-S20-S21-H21-S27-H23-S29-H15 in domain II. The C terminus of H25 and the N terminus of H15 connect the two domains.

Table S1. Statistics of data collection and phasing

	Native	$HgCl_2$ derivative
Data collection		
Space group	$P2_12_12_1$	$P2_12_12_1$
Cell constants (*a*, *b*, *c*)	57.6, 90.7, 240.4	58.3, 91.4, 243.4
Total/unique reflections	254,664/53,248	289,631/74,651*
R_s†	6.2 (50.3)	6.9 (40.9)
Resolution, Å	20–2.35	20–2.62
Completeness, %	99.4 (98.8)	98.4 (91.1)
$(I)/(\sigma I)$	20.2 (3.0)	16.1 (2.6)
Phasing by AutoSol		
No. of Hg		8
Figure of merit		0.22
Estimated map CC		0.39±0.11
R factor (FC vs FP)		0.29
rms (FH)/rms (E)		0.63
Refinement		
Model R/R_{free} factor,‡ %	22.6/27.3	
No. of molecules/ASU	2	
No. of residues	109–630 in chain X and Y	

Numbers in brackets denote the values found in the highest resolution shell. CC, correlation coefficient; FC, calculated structure factor; FP, protein structure factor; FH, heavy atom structure factor; ASU, asymmetric unit.

*Friedel mates were treated as independent reflections.

†$R_s = \Sigma_h\Sigma_i|I_i(h) - \langle I(h)\rangle|/\Sigma_h\Sigma_i I_i(h)$; where *i* are the independent observations of reflection *h*.

‡The R_{free} factor was calculated from 5% of the data, which were removed at random before the refinement was carried out.

Table S2. Statistics on data collection and structure refinement

	Native-FeS domain
Data collection	
Space group	$P2_12_12_1$
Cell constants (*a*, *b*, *c*)	70.5, 91.2, 252.9
Total/unique reflections	339,176/83,472
R_s*	5.3 (50.8)
Resolution, Å	35–2.20
Completeness, %	99.6 (99.7)
$(I)/(\sigma I)$	16.0 (2.7)
Refinement	
Model R/R_{free} factor,† %	22.0/26.0
No. molecules/ASU	2
No. of residues	3–630 in chain X 108–629 in chain Y
B factors, Å^2	
Overall	54
N-terminal domain	107
rms deviation from ideal geometry	0.0071.849
Bonds, Å	
Angles, °	
Ramachandran statistics, %	
Most favored/generously allowed/disallowed regions	97.5/2.5/0

Numbers in brackets denote the values found in the highest resolution shell. ASU, asymmetric unit.

*$R_s = \Sigma_h\Sigma_i|I_i(h) - \langle I(h)\rangle|/\Sigma_h\Sigma_i I_i(h)$; where *i* are the independent observations of reflection *h*.

†The R_{free} factor was calculated from 5% of the data, which were removed at random before the refinement was carried out.

Table S3. Structural comparison of RACo with members of the ASKHA (acetate and sugar kinases/heat shock protein 70/actin) family

		RACo	3L6Q	1E4G	3QBW	1H1V	1HUX
RACo	identity, %	—	15	12	10	10	10
	rmsd, Å	—	3.8	5.2	4.9	4.4	3.9
	Z score	—	12.2	13.6	14.1	11.8	12.0
3L6Q	identity, %	15	—	13	13	13	15
	rmsd, Å	3.8	—	3.2	4.5	2.6	3.0
	Z score	12.2	—	19.7	13.1	25.8	16.0
1E4G	identity, %	12	13	—	11	12	16
	rmsd, Å	5.2	3.2	—	4.4	3.4	3.6
	Z score	13.6	19.7	—	14.2	21.1	16.5
3QBW	identity, %	10	13	11	—	11	13
	rmsd, Å	4.9	4.5	4.4	—	5.11	4.0
	Z score	14.1	13.1	14.2	—	1.2	17.9
1H1V	identity, %	10	13	12	11	—	15
	rmsd, Å	4.4	2.6	3.4	5.1	—	3.8
	Z score	11.8	25.8	21.1	11.2	—	14.9
1HUX	identity, %	10	15	16	13	15	—
	rmsd, Å	3.9	3.0	3.6	4.0	3.8	—
	Z score	12.0	16.0	16.5	17.9	14.9	—
Average	identity, %	11.4	13.8	12.8	11.6	12.2	13.8
	rmsd, Å	4.4	3.4	4.0	4.6	3.9	3.7
	Z score	12.7	17.4	17.0	14.1	17.0	15.5

The structure of RACo was compared with the N-terminal domain of Hsp70 from *Cryptosporidium parvum* (PDB ID 3L6Q), FtsA from *Thermotoga maritime* (PDB ID 1E4G; ref. 1), 1,6-anhydro-*N*-acetylmuramic acid kinase (ANMK, PDB ID 3QBW; ref. 2), Gelsolin G4-G6/Actin complex (PDB ID 1H1V; ref. 3), and component A of (*R*)-2-hydroxyglutaryl-CoA dehydratase from *Acidaminococcus fermentans* (PDB ID 1HUX; ref. 4).

1. Van den Ent F, Lowe J (2000) Crystal structure of the cell division protein FtsA from Thermotoga maritima. *Embo J* 19:5300–5307.
2. Bacik JP, et al. (2011) Molecular basis of 1,6-anhydro bond cleavage and phosphoryl transfer by Pseudomonas aeruginosa 1,6-anhydro-N-acetylmuramic acid kinase. *J Biol Chem* 286:12283–12291.
3. Choe H, et al. (2002) The calcium activation of gelsolin: insights from the 3A structure of the G4-G6/actin complex. *J Mol Biol* 324:691–702.
4. Locher KP, et al. (2001) Crystal structure of the Acidaminococcus fermentans 2-hydroxyglutaryl-CoA dehydratase component A. *J Mol Biol* 307:297–308.

Table S4. Structural comparison of RACo with plant-type [2Fe-2S] ferredoxins

		RACE	1FRD	1OFF	1RFK	2PVG	1AWD
RACE	identity, %	—	28	29	30	29	29
	rmsd, Å	—	1.9	1.9	2.0	2.0	2.1
	Z score	—	13.8	13.7	13.5	13.5	13.3
1FRD	identity, %	28	—	56	54	56	62
	rmsd, Å	1.9	—	0.7	0.7	0.6	0.7
	Z score	13.8	—	21.1	21.8	21.1	20.6
1OFF	identity, %	29	56	—	80	99	75
	rmsd, Å	1.9	0.7	—	0.6	0.4	0.4
	Z score	13.7	21.1	—	21.9	22.4	22.0
1RFK	identity, %	30	54	80	—	79	73
	rmsd, Å	2.0	0.7	0.6	—	0.6	0.5
	Z score	13.5	21.8	21.9	—	21.8	21.5
2PVG	identity, %	29	56	99	79	—	74
	rmsd, Å	2.0	0.6	0.4	0.6	—	0.5
	Z score	13.5	21.1	22.4	21.8	—	21.8
1AWD	identity, %	29	62	75	73	74	—
	rmsd, Å*Z* score	2.1	0.7	0.4	0.5	0.5	—
		13.3	20.6	22.0	21.5	21.8	—
Average	identity, %	29.0	51.2	67.8	63.2	67.4	62.6
	rmsd, Å	2.0	0.9	0.8	0.9	0.8	0.8
	Z score	13.6	19.7	20.2	20.1	20.1	19.8

For the comparison the structures of the ferredoxin from *Anabena 7120* (PDB ID 1FRD; ref. 1), [2Fe-2S] ferredoxin from *Synechocystis* sp. Pcc 6803 (PDB ID 1OFF; ref. 2), ferredoxin from *Mastigocladus laminosus* (PDB ID 1RFK; ref. 3), the binary complex between ferredoxin and ferredoxin:thioredoxin reductase (PDB ID 2PVG; ref. 4), and ferredoxin from *Chlorella fusca* (PDB ID 2PVG; ref. 5) were used

1. Jacobson BL, Chae YK, Markley JL, Rayment I, Holden HM (1993) Molecular structure of the oxidized, recombinant, heterocyst [2Fe-2S] ferredoxin from Anabaena 7120 determined to 1.7 Å resolution. *Biochemistry* 32:6788–6793.
2. Van den Heuvel RH, et al. (2003) The active conformation of glutamate synthase and its binding to ferredoxin. *J Mol Biol* 330:113–128.
3. Fish A, Danieli T, Ohad I, Nechushtai R, Livnah O (2005) Structural basis for the thermostability of ferredoxin from the cyanobacterium Mastigocladus laminosus. *J Mol Biol* 350:599–608.
4. Dai S, et al. (2007) Structural snapshots along the reaction pathway of ferredoxin-thioredoxin reductase. *Nature* 448:92–96.
5. Bes MT, et al. (1999) Crystal structure determination at 1.4 Å resolution of ferredoxin from the green alga Chlorella fusca. *Structure* 7:1201–1211.